SIMULATION OF CARGO CONTAINER INTERROGATION BY D-D NEUTRONS

Tak Pui Lou
Lawrence Berkeley National Laboratory, California 94720
TPLou@LBL.gov

Arlyn Antolak
Sandia National Laboratories, California 94551
Antolak@sandia.gov

ABSTRACT

High fidelity, three-dimensional computer models based on a CAD drawing of an intermodal cargo container, representative payload objects, and detector array panels were developed to simulate the underlying physical events taking place during active interrogation. These computer models are used to assess the performance of interrogation systems with different sources and detection schemes. In this presentation, we will show that the use oversimplified models, such as analyzing homogenized payloads only, can lead to errors in determining viable approaches for interrogation.

Keywords: active interrogation; deuterium; neutron; transport modeling
PACS: 24.10.Lx; 02.70.Uu; 28.20.-v

1. INTRODUCTION

Active interrogation of nuclear material hidden in cargo containers has become an important research topic for homeland security. Active interrogation involves probing a container with highly penetrating particles such as neutrons or photons to induce fission in the nuclear material and subsequently detect the emitted fission signals (secondary neutrons and gammas). Generally, a neutron source is used when strong photon-absorbing cargo (e.g., thick metal materials) or shielding is present, and a photon source is used when strong neutron-absorbing (e.g., hydrogenous materials) shielding or payload material is present. The fission-induced radiations that could be detected are either prompt (instantaneously emitted) or delayed (up to 100 seconds) neutrons and gamma-rays. Much attention has focused on using the delayed gamma-ray signal for active interrogation because these gammas can emerge from a cargo-laden container to be detected and their yield per fission event is relatively high. Because cargo containers have very diverse and complex cargos, one must rely on modeling and simulation to assess the utility of a proposed active interrogation system. Systems based on delayed gamma counting have been favored because models predict that neutron counting would fail if the nuclear material was hidden in thick hydrogenous cargo. However, we find that in many instances the oversimplified models failed to take into account the characteristics of the usual cargo that would be inspected. To overcome some of these deficiencies, we have developed very high fidelity models of the cargo container itself as well as representative cargo payloads. Simulations using these models more accurately account for the underlying physical events that can occur during particle

transport. The performance of the interrogation system can then be optimized more accurately. For example, we show the importance of incorporating a neutron counting scheme and that the background of a delayed gamma counting scheme should not be neglected in neutron-based interrogation systems.

Some active interrogation techniques propose detecting the high-energy delayed gamma signal from fission,[1,2] but defining and extracting the background radiation in a measurement can be very difficult. The reason is that counting these gammas is not foolproof especially when the system is based on a D-T neutron source due to its high (n,γ), (n,n'γ) and (n,xγ) activation of surrounding materials. Although decay gammas from activation using a photon interrogation source is expected to be lower, it is still important to improve the signal-to-background ratio by selecting only high-energy gammas from fission products with specific half-lives.[3] While our analysis is presently limited to prompt gammas only, the results obtained using a D-D neutron-based source suggests one should not rely only on detecting delayed gamma but, instead, more reliable interrogations will be made using both delayed gamma and prompt neutron signals.

2. COMPUTATIONAL APPROACH

The Monte Carlo N-Particle eXtended (MCNPX) code was chosen for our modeling and simulation effort because it has a broad range of features in terms of its validated physics models, extensive nuclear databases, parallel computation capability and the ability to handle complex geometries.[4] A very detailed model of the cargo container has been developed based on computer-aided design (CAD) drawings of an actual International Standard Organization (ISO) cargo container.[5] We have also developed five cargo payload models consisting of oak wood, glass-bottled water, laptop computers, automobile engines, and a block of borated polyethylene. The usual configuration is the payload material fills the cargo container sitting inside a room with concrete floor and walls. The concrete room has an internal space of ~12×16×8 m^3. A point neutron source is located at the center of the room and is positioned 1.4 meters above the concrete floor. The walls and ceiling are assumed to be 1 meter thick of concrete and the simulations take into account any scattered signals from these surfaces.

2.1. ISO Cargo Container Model

The cargo container is located a half meter from the point neutron source and has a capacity of ~6×2×2 m^3 for its payload volume. Figure 1 shows the container model rendered with MCNPVISED and composed by GIMP.[6,7] The model includes detailed features of the container such as the corrugated panels, corner posts, corner fittings, rails, forklift pockets, plywood floor, etc. The container has an empty (tare) weight of 2,200 kg and its payload has a weight limit of 28,280 kg. For the active interrogation simulations, we used an 8-kg sphere of uranium located at the center of the container. Steels with different compositions are used for different parts of the container to ensure the best accuracy in the simulation results. Table I lists most of the material compositions and densities used in the container model as well as the material compositions used in the payload models. For materials that are not listed, they are either pure elements or their compositions are described separately in the following sections.

Table I Material composition used in the computer model

Material	Composition (atomic fraction %)	Density (g/cm^3)
Oakwood	$^{Nat}C_6$ $^{1}H_{9.99885}$ $^{2}H_{.00115}$ $^{16}O_{4.98785}$ $^{17}O_{0.0019}$ $^{18}O_{0.01025}$	0.7
Plywood		0.5
SPA-H steel	^{Nat}C (0.55064) ^{28}Si (1.35742) ^{29}Si (0.06893) ^{30}Si (0.04544) ^{55}Mn (0.50160) ^{31}P (0.26691) ^{32}S (0.06895) ^{63}Cu (0.35995) ^{65}Cu (0.16044) ^{50}Cr (0.05757) ^{52}Cr (1.11017) ^{53}Cr (0.12588) ^{54}Cr (0.03134) ^{58}Ni (0.41552) ^{60}Ni (0.16006) ^{61}Ni (0.00696) ^{62}Ni (0.02218) ^{64}Ni (0.00565) ^{54}Fe (5.53430) ^{56}Fe (86.87672) ^{57}Fe (2.00636) ^{58}Fe (0.26701)	7.85
SS490 steel	^{Nat}C (1.01145) ^{28}Si (0.45335) ^{29}Si (0.02302) ^{30}Si (0.01517) ^{55}Mn (1.40720) ^{31}P (0.06240) ^{32}S (0.06909) ^{54}Fe (5.66721) ^{56}Fe (88.96314) ^{57}Fe (2.05455) ^{58}Fe (0.27342)	
SM490A steel	^{Nat}C (0.92071) ^{28}Si (0.99868) ^{29}Si (0.05071) ^{30}Si (0.03343) ^{55}Mn (1.61035) ^{31}P (0.06248) ^{32}S (0.06918) ^{54}Fe (5.62607) ^{56}Fe (88.31732) ^{57}Fe (2.03963) ^{58}Fe (0.27144)	
SCW49 steel (cast steel)	^{Nat}C (1.00658) ^{28}Si (1.44373) ^{29}Si (0.07331) ^{30}Si (0.04833) ^{55}Mn (1.50045) ^{31}P (0.07097) ^{32}S (0.06875) ^{63}Cu (0.35891) ^{65}Cu (0.15997) ^{50}Cr (0.02296) ^{52}Cr (0.44278) ^{53}Cr (0.05021) ^{54}Cr (0.01250) ^{58}Ni (0.31870) ^{60}Ni (0.12276) ^{61}Ni (0.00534) ^{62}Ni (0.01702) ^{64}Ni (0.00433) ^{54}Fe (5.51022) ^{56}Fe (86.49870) ^{57}Fe (1.99763) ^{58}Fe (0.26585)	
Air	^{Nat}C (0.01502) ^{14}N (78.44743) ^{16}O (21.01933) ^{17}O (0.00801) ^{18}O (0.04319) ^{Nat}Ar (0.46702)	1.293×10^{-3}
Concrete	^{16}O (56.18138) ^{17}O (0.02140) ^{18}O (0.11545) ^{28}Si (18.74395) ^{29}Si (0.95177) ^{30}Si (0.62742) ^{Nat}Ca (1.85946) ^{27}Al (2.13429) ^{23}Na (2.13651) ^{1}H (16.80183) ^{2}H (0.00193) ^{54}Fe (0.02482) ^{56}Fe (0.38959) ^{57}Fe (0.00900) ^{58}Fe (0.00120)	2.3
Yellow-green glass	^{28}Si (21.75948) ^{29}Si (1.10489) ^{30}Si (0.72835) ^{Nat}Ca (4.33345) ^{23}Na (6.83999) ^{Nat}C (3.41685) ^{54}Fe (0.00212) ^{56}Fe (0.03327) ^{57}Fe (0.00077) ^{58}Fe (0.00010) ^{16}O (61.63060) ^{17}O (0.02348) ^{18}O (0.12665)	2.536
Water	^{16}O (33.17708) ^{17}O (0.01264) ^{18}O (0.06818) ^{1}H (66.49893) ^{2}H (0.00762) ^{Nat}C (0.00015) ^{14}N (0.00005) ^{Nat}Ca (0.20929) ^{23}Na (0.02606)	0.997
Compact disc	^{Nat}C (48.61273) ^{1}H (42.24832) ^{2}H (0.00484) ^{16}O (9.10228) ^{17}O (0.00347) ^{18}O (0.01870) ^{27}Al (0.00966)	1.2
Low density polyethylene	^{Nat}C $^{1}H_{1.99977}$ $^{2}H_{0.00023}$	0.016
Li ion battery	^{Nat}C (50.00000) ^{1}H (19.22855) ^{2}H (0.00221) ^{16}O (13.42883) ^{17}O (0.00511) ^{18}O (0.02760) ^{19}F (11.53846) ^{31}P (1.92308) ^{59}Co (1.92308) ^{6}Li (0.14596) ^{7}Li (1.77712)	2.382
Fictitious laptop screen	^{28}Si (5.76436) ^{29}Si (0.29270) ^{30}Si (0.19295) ^{Nat}C (37.50000) ^{1}H (37.49568) ^{2}H (0.00431) ^{16}O (18.70444) ^{17}O (0.00712) ^{18}O (0.03844)	0.779
Hard disc platter	^{27}Al (93.33333) ^{54}Fe (0.38967) ^{56}Fe (6.11693) ^{57}Fe (0.14127) ^{58}Fe (0.01880)	2.631
HEU	^{235}U (90) ^{238}U (10)	18.84

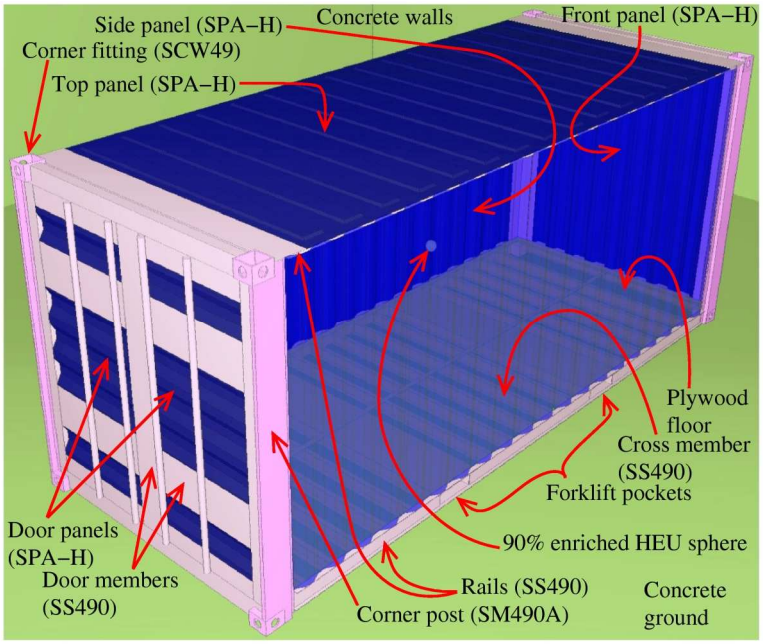

Figure 1 A 20'×8'×8.5' dry freight ISO cargo container

2.2. Payload Models

Five different kinds of cargo payloads were studied: two representing homogenous cargos and three representing heterogeneous cargos. The two homogeneous models are oak wood and borated polyethylene. Oak wood is modeled by having the cargo container completely filled with 0.7 g/cm^3 cellulose. For the second model, we used a 2.4×2.4×2.4 m^3 cube of 1.2 g/cm^3 borated polyethylene consisting of 32 wt/% boron-10 and 68 wt/% of polyethylene situated at the center of the container.

The first (heterogeneous) model is of a laptop computer inside its cardboard shipping box. The laptop consists of three different layers of (smeared) material components: a hard disc platter, copper heat sink and a lithium-ion battery. (See Figure 2) The densities and material compositions for the screen layer and hard disc platter are listed in Table I. The layer representing the computer motherboard is silicon dioxide with a trace amount of gold and has a density of 2.4 g/cm^3. The remaining layer consists of polyethylene with a density of 0.5 g/cm^3 and the copper heat sink with a density of 3 g/cm^3. The densities are chosen in such a way that the mass is equal to typical weight of these components. The composition of the power supply is 50% iron plus 50% copper and the unit weighs 250 g. The power cords and cables are approximated by two polyethylene rods with density of 0.92 g/cm^3. Both the paper box and cardboard paper divider have the same composition as plywood but their densities are chosen to be 0.5 g/cm^3 and 0.6 g/cm^3 respectively. The outside dimensions of the paper box are 39×16×34 cm^3. Each boxed laptop weighs 5.6 kg and a total of (15×14×7=) 1,470 laptops are loaded into one cargo container.

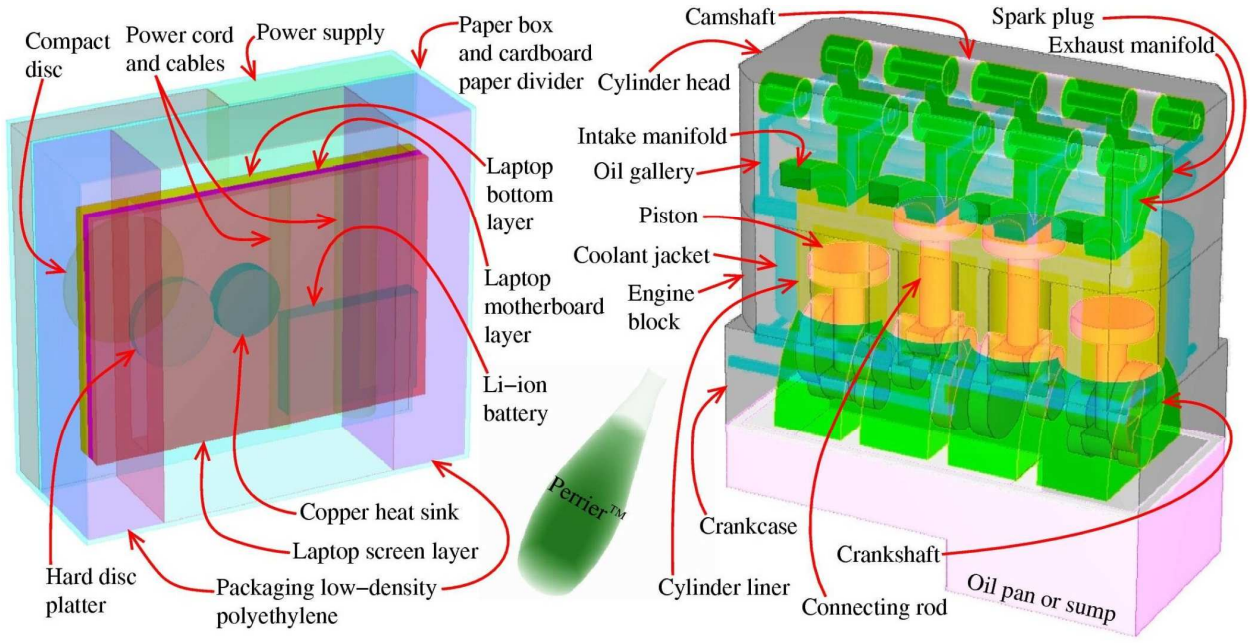

Figure 2 Heterogeneous payload models: computer laptop in a box, glass bottled water, and engine

We have also developed a model of packaged bottled water. The bottle is 26 cm tall and its largest diameter is 9 cm. The model is created in MCNPX using combinations of ellipsoids, cones and cylinders. The thickness of the bottle is obtained by adjustment of the inner ellipsoid, cone and cylinder until the calculated mass from the model matches the measured mass of a commercially available water bottle (i.e. ~430 g). The cargo container can be filled with 14,175 bottles (or 9×5×3= 135 cases) of water.

The remaining heterogeneous payload model is of an inline four-cylinder engine found in a typical imported gasoline automobile. Each engine weighs ~144 kg and has an overall dimension of 20×46×46 cm^3 as shown in Figure 2. Because iron has a very high inelastic scattering cross section for neutrons and different kinds of engine blocks are made of different alloys, our model assumes the whole engine is made of cast steel to provide a more conservative estimate in the simulations. There are (7×5×5=) 175 engines stacks inside the middle 1.5 m of the container with each engine separated from its neighbor by by ~2 cm.

2.3. Detector Panels Model

The interrogation system model also includes two sets of detector panel frameworks: one on the source side and one on the far side of the container. A simplified detector panel framework is used to determine the expected numbers of photons or neutrons that strike the detector (see Figure 3). Unlike the detectors on the far side of the container, the source side has the center panel removed to allow the neutron source to operate from that location. Both sets of detector panels are a half centimeter away from the side panels of the container and tallies are made at ~4 cm away from the side panels. Each panel can be filled with three different kinds of detectors in

a tricusp pattern. Currently, the detector panel framework is not filled with any material and is used only for defining the regions where neutron and gamma detectors will be placed.

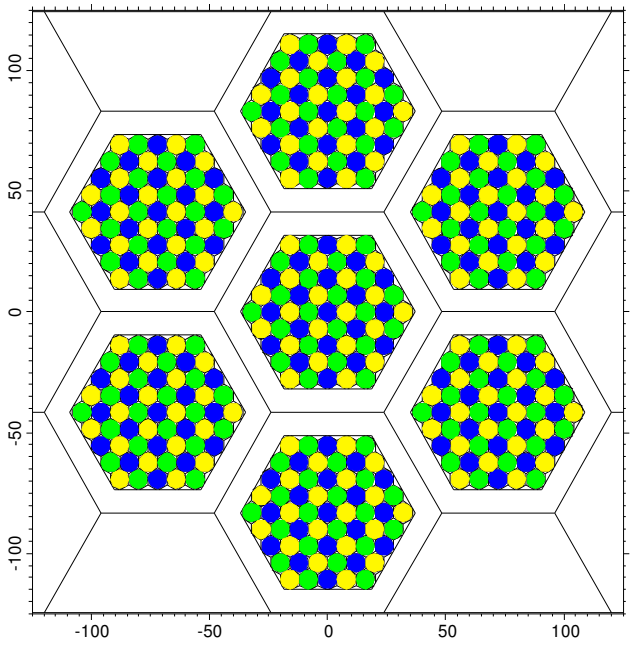

Figure 3 Detector panels (scales are in centimeter)

2.4. Other General Assumptions

The source neutrons are produced with the beam directed perpendicularly to the cargo container's side wall with the source 50 cm from the wall. For a typical D-D neutron generator, the neutron energy will depend on the angle of emission with a maximum energy of 2.78 MeV in the forward direction (i.e. 0°), and a minimum energy of 2.18 MeV at its backward angle (i.e. 180°). All source neutrons are assumed to be emitted at time zero.

Several quantities are tallied in the simulations including the induced fission rate, neutron production rate, (n,2n) reaction rate, (n,3n) reaction rate, fission neutron yields and neutron lifetimes. The fission neutron yields (nubar) are sampled from a Gaussian distribution. Neutrons are transported in analog mode with explicit capture as implicit capture imposed. If implicit capture was adopted, the Monte Carlo calculation will spend more computer time on sampling the less important low-energy neutrons. We are in favor of performing analog transport calculation because we plan to make use of the energy deposition tally and pulse height tally in our future work with these computer models. The current release version of MCNPX prohibits the use of energy deposition tally and pulse height tally in non-analog transport mode. The neutron current at the detector panels is tallied with six energy bins and six time bins as listed in Table II. The gamma current tallies use the same time binning as the neutron current tallies but the gamma current tallies have more energy bins to help distinguish discrete gamma lines from the gammas with continuum distribution. These energy bins were chosen manually so that they

bound some of the intense gamma lines from neutron interactions with materials defined in the computer model.

Table II Neutron energy bins and time bins for the current tally

Energy	0.625 eV	100 eV	100 keV	2.8 MeV	8 MeV	20 MeV
Time	10 ns	100 ns	1 μs	5 μs	100 μs	10^{29} s

3. RESULTS

For an active interrogation system, the most important parameters are the number (counts) of detectable signals and signal-to-background ratio. There are two common ways to improve signal-to-background ratio: time and energy discriminations of the detected signals. These two discriminating parameters can be applied separately but they usually work best when both are applied together. As mentioned earlier, the fission-induced signals from nuclear materials that could be detected are prompt gammas, delayed gammas, prompt neutrons and delayed neutrons. The MCNPX version used in our simulations does not have the capability to compute the delayed gamma-ray distribution. We found that the gamma background (due to activation) is orders-of-magnitude higher than the prompt fission gamma signals, thus rendering this signal not attractive.

Our simulations did include both prompt and delayed neutrons signals. However, the delayed neutron fractions for most common nuclear materials are less than 1% (e.g. 0.685 % for thermal neutron fission of ^{235}U) and their average neutron energies are hundreds of keV (e.g. 405 keV for ^{235}U). As a result, delayed neutrons contribute very little to the detectable signal in an active interrogation scenario and the neutron current tallies at the detector are actually only a measure of the prompt fission neutrons, although delayed neutrons are included in the simulations. The simulation results of the neutron current tallies for the heterogeneous payloads are shown in Figure 4.

It is evident that fast neutrons which hit the detector panels from the source have energies less than 100 keV within 100 μs after they are born. Thus, any fast neutrons detected after 100 μs could only come from the nuclear material in the container or from natural background. (Note: while there is no other time bin between 5 μs and 100 μs, it should be possible to gate the detector with shorter off time like 20 μs.) Since the fast neutron background at sea level is expected to be less than 3×10^{-3} n/cm^2-s,[8] the number that hit a detector panel would be less than 12 n/s. Figure 4 shows that the minimum number of fast fission neutrons that hit a single detector panel in our three heterogeneous model scenarios is greater than 5×10^{-9} neutrons per source neutron. Thus, a neutron source having an intensity of $\geq5\times10^{10}$ n/s would have a fast fission neutron signal-to-background ratio better than 20:1.

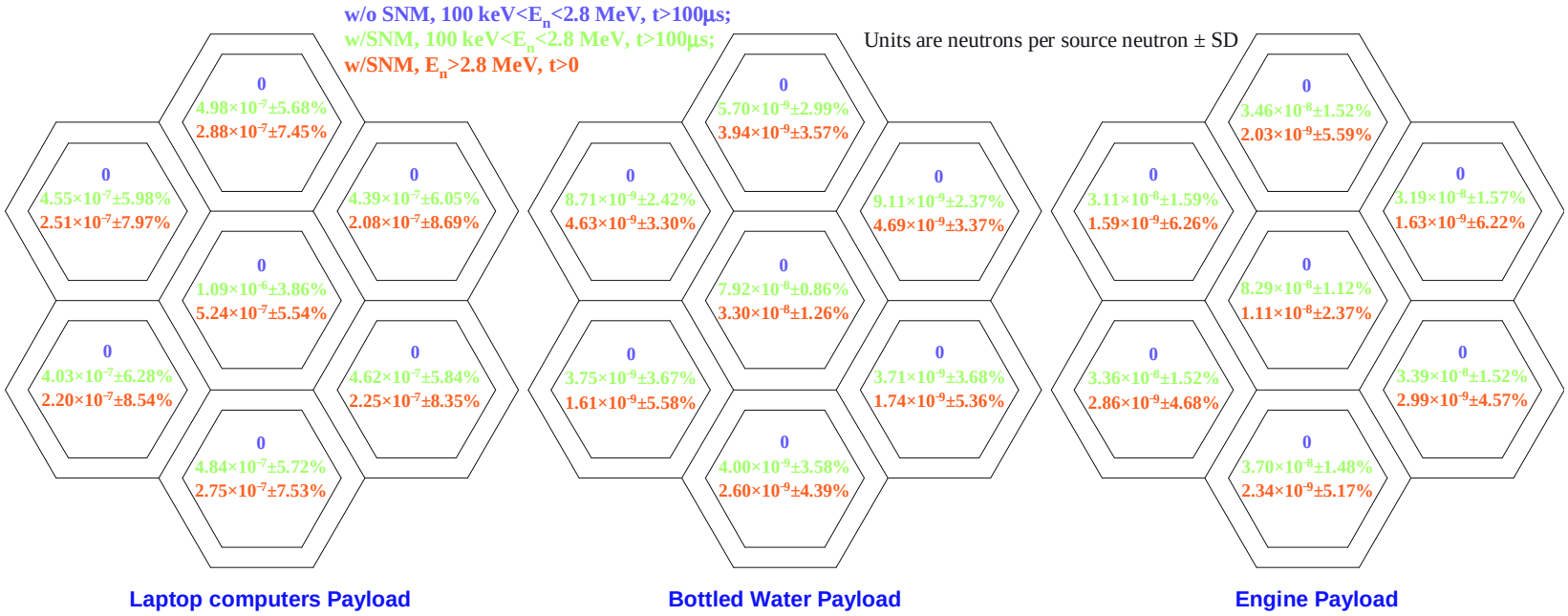

Figure 4 Neutron currents at the detector panels for different payloads

Unlike the large signal-to-noise ratio and copious amount of fast fission neutrons leaking out of the cargo container in the heterogeneous hydrogenous (bottled water) model, simulations with homogeneous hydrogenous payloads (oak wood and borated polyethylene) show that the fast fission neutron signal cannot be detected. Table III lists the fission rates for each payload model as well as two extra payloads which were simulated for comparison purposes: a homogenous steel cube with a density and total volume equivalent to the engine model (i.e. ~3 g/cm^3 and ~2×2×2 m^3) and a polyethylene cube having a density of ~0.8 g/cm^3.

Table III Induced fission rate for different payloads

Oak wood	Laptop computers	Bottled water	Engine	Smeared steel cuboid	Borated polyethylene[†]	Polyethylene w/o boron[†]
1.8×10^{-6}	4.3×10^{-4}	1.2×10^{-4}	2.1×10^{-4}	2.0×10^{-4}	5.4×10^{-11}	9.4×10^{-9}

4. DISCUSSION

Our simulation results show that D-D neutron interrogation works well except when the payload consists of thick uniform hydrogenous material. This is expected as hydrogenous materials are strong neutron absorbers and have very high moderation power. Once a source neutron becomes thermalized, it will very likely be trapped locally and get absorbed before a fission event can occur. Even if fission events can occur, the fission neutrons lose so much energy on their way back out that it is impossible to distinguish them from other thermalized source neutrons. On the other hand, the bottled water (i.e. heterogeneous hydrogenous payload) scenario shows that the empty space between each bottle provides (streaming) flight paths almost completely free from collisions and ,thereby, makes fast fission neutron counting possible. The steel cube model shows that a homogeneous non-hydrogenous payload does not have a significant effect on fission rate and detectable signals. In fact, the fission rate of the steel cube model is only 5 % less than that of the (heterogeneous) engine model, and the fast fission neutron signals are very similar.

Since a fast fission neutron detection scheme fails for the thick uniform hydrogenous payload, we considered a counting scheme for fission-induced gamma-rays. As mentioned earlier, the prompt gammas cannot be used because their intensity is several orders-of-magnitude lower than the activation background. Energy and time discrimination methods are a possibility, but these techniques cannot improve the signal-to-background ratio because there are not many intense high-energy gamma lines. Therefore, the only remaining option is to use the delayed gamma signal. The drawback to the latter approach is that D-D neutrons (~2.5 MeV average energy) are not penetrating enough to cause adequate fission in a reasonable counting time for hydrogenous materials (e.g. oak wood, polyethylene or borated polyethylene).

An alternative option is to use a higher energy (e.g. D-T) neutron source for interrogating the cargo container. Although with a higher energy neutron source one gains in penetrability, the

[†] The neutron source is 23.82 cm away from the container side panel instead of a half meter and the detector panel is 20 cm away from the container side panel for the polyethylene and borated polyethylene cases.

problem is that the average energy of the prompt fission neutrons is ~2 MeV so they cannot make their way out of a container if it is filled with homogenous hydrogenous material. When the D-D neutron source is replaced with a D-T neutron source, the fission rate is 1.3×10^{-6} fission per source neutron in the polyethylene scenario and practically no fission neutrons can leak out of the container. Nevertheless, this fission rate is high enough to allow delayed gamma-rays counting in a reasonable inspection time. On the other hand, the 14-MeV neutrons from a D-T source also lead to a large gamma-ray background which interferes with the delayed gamma signal one is trying to detect. For example, the $^{16}O(n,p)$ reaction at a threshold energy of about 10-MeV produces ^{16}N which decays with a half-life that falls in the same delayed gamma counting time window. In this case, D-D neutrons have an advantage of having no such background because their energy is well below the threshold energy for this reaction. The prompt gammas tallied in the simulations show that the background for the detectors on the source side can be ~30 times higher than the detectors on the opposite side of the container. We also found that the fission rate calculated with borated polyethylene shielding is ~30 times less compared to the polyethylene without boron. Thus, the background caused by the D-T source activation of surrounding materials can be up to 200 times higher than the fission gamma signal implying that this source would be ineffective for dense homogeneous-hydrogenous cargo.

5. CONCLUSION

High fidelity simulations show that a 2.5-MeV D-D neutrons provide viable interrogation of cargo containers with normal payloads, but are less useful when thick hydrogenous materials are present. For the latter case, a 14-MeV D-T neutron source cannot be considered as a straightforward solution in terms of its increased penetrability alone. To address this issue, we have started to analyze high-energy photon sources for interrogation and will use the same detailed computational models to predict their performance for detecting useful signals. Preliminary indications are that using the combination of a high-energy photon source and a D-D neutron source will be most effective system for inspecting cargo containers.

ACKNOWLEDGEMENTS

This work was performed as work for others by the US Department of Homeland Security, Domestic Nuclear Detection Office, Office of Transformational Research and Development under the auspices of the U.S. Department of Energy by Lawrence Berkeley National Laboratory under contract number DE-AC02-05CH11231 and by Sandia National Laboratories, a multiprogram laboratory operated by Sandia Corporation, a Lockheed Martin Company, for the United States Department of Energy's National Nuclear Security Administration under contract DE-AC04-94AL85000. This work used computational resources of the National Energy Research Scientific Computing Center which is supported by the Office of Science of the U.S. Department of Energy under Contract No. DE-AC02-05CH11231.

The authors thank Mr. Bob Welsch from Sea Box, Inc. for providing the CAD drawing of the ISO cargo container and, also, Mr. Michael King, LBNL for useful technical discussions.

REFERENCES

1. E.B. Norman, S.G. Prussin, R.-M. Larimer, et al., Nuclear Instruments and Methods in Physics Research A, **521**, pp. 608-610, (2004).
2. J. Pruet, M.-A. Descalle, J. Hall, et al., Journal of Applied Physics, **97**, 094908-1, (2005).
3. Plukis, D. Ridikas, F. Damoy, et al., Proceeding of the International Workshop on Neutron Measurements, Evaluations and Applications NEMEA-2, Bucharest, pp. 137-140, (2004).
4. MCNPX User's Manual edited by D.B. Pelowitz, (2005).
5. K.C.E., proprietary CAD drawing from Sea Box, Inc., (1998).
6. MCNP Visual Editor <http://www.mcnpvised.com>, (2006).
7. GIMP – The GNU Image Manipulation Program <http://www.gimp.org>, (2007).
8. M.I. Frank, S.G. Prussin, P.F. Peterson, et al., Journal of Radioanalytical and Nuclear Chemistry, **249**, No. 1, pp. 145-151, (2001).